

## Photoionization and Photodissociation Processes of Multiply-Charged Cytochrome c Ions Produced by Electrospray Ionization

Shinji NONOSE, Hiroaki TANAKA, and Kiyokazu FUKU  
*Department of Chemistry, Faculty of Science, Kobe University*

### Abstract

Photo-induced reactions of multiply-charged cytochrome c ions,  $(M + nH)^{n+}$  ( $n = 9 - 17$ ) are investigated at 28200 and 18800  $\text{cm}^{-1}$  by using a tandem mass spectrometer with electrospray ionization source. Photoionization is found to be the dominant process for the lower charged states ( $n = 9 - 12$ ) and its yield decrease rapidly with increasing the charge. The photoionization is ascribed to the emission of electron by multiphoton excitation of heme under the influence of Coulomb attractive potential arising from the charges in the polypeptide chain. Model calculations of the Coulomb potential suggest that the structure of the polypeptide chain is completely elongated.

**Key Words:** Electrospray ionization; Photoionization; Cytochrome c ions; Coulomb potential; Conformations of protein ions

### 1. Introduction

The structures and reactions of gas-phase clusters have been studied extensively using various spectroscopic methods in order to bridge the gap between the gas phase and the condensed phase [1-4]. For examples, our group and Schulz's group have investigated the electronic structures of the clusters such as metal atoms and/or ions solvated with polar molecules for modeling microscopic solvation [5-12]. Recent advances in electrospray ionization (ESI) allow us to produce various kinds of nonvolatile molecules in the gas phase without destruction [13,14]. The ESI mass spectrometry is now routinely used for sensitive analytical determination of biological molecules, accurate measurement of molecular weights and sequence information. Several groups have applied ESI to the spectroscopic studies of gas-phase cluster ions [15-18]. These studies provide information on the microscopic solvation and the reaction dynamics of gas-phase clusters.

The conformations of large biological molecules such as proteins in the condensed phase are strongly influenced by surrounding solvent environments. In order to investigate the intra- and intermolecular interactions, nonvolatile molecules should be introduced into the gas phase as ions. The gas phase is an unusual environment for the investigation of biological molecules. However, the gas-phase studies are expected to provide a deeper understanding of the intramolecular interactions as well as hydration interactions that determine the conformations. Several different techniques have been employed to obtain information about the conformations of large biological molecules in the gas phase. McLafferty, Williams, and their collaborators have examined electron-capture kinetics [19], H/D exchange kinetics [20], proton-transfer kinetics [21], or blackbody infrared radiative dissociation [22].

Jarrold and coworkers have performed ion mobility measurements to study the geometries of naked protein ions in the gas phase [23-25]. Smith and coworkers have investigated the collision-induced-dissociation processes of multiply-charged protein ions [26-29].

In the present work, the photo-induced reactions of multiply-charged cytochrome c ions prepared by ESI are investigated with mass spectrometry. Cytochrome c is a relatively small protein and has an iron-containing heme group covalently bound to two cysteines in a polypeptide chain of ~100 residues. Since there are no disulfide bridges in cytochrome c, it is free to adopt conformations that are quite different from the native conformations. We measure the photoionization yields at 28200 and 18800  $\text{cm}^{-1}$  for the charge-selected cytochrome c ions,  $(M + nH)^{n+}$  ( $n = 9 - 17$ ). Based on these results, we discuss the mechanisms of the photoionization and photodissociation of heme in relation to the protein conformations.

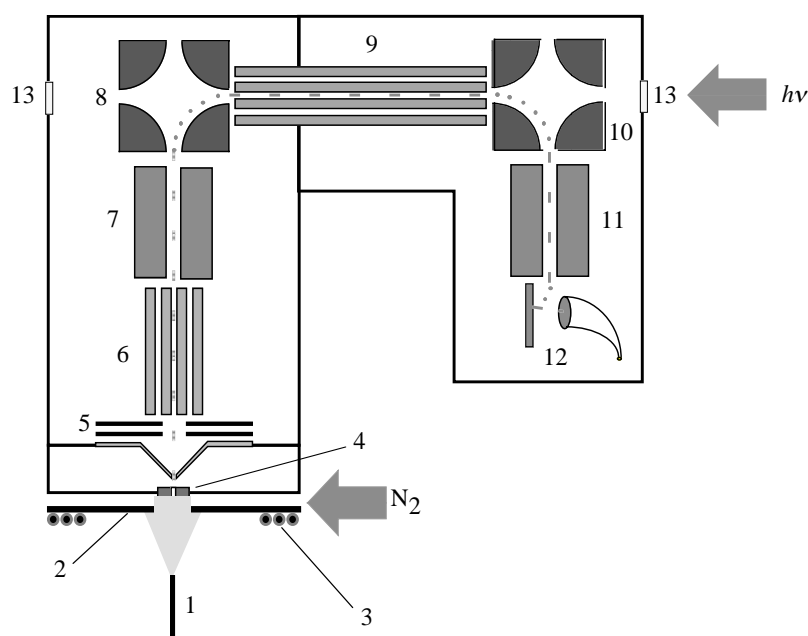


**Fig. 1.** Schematic diagram of the tandem mass spectrometer with ESI source; (1) electro spray needle movable via three axis positioner, (2) interface plate, (3) heater, (4) aperture (0.1 mm i.d.), (5) skimmer and electrostatic lenses, (6) first octapole ion-beam guide (OPIG1), (7) first quadrupole mass filter (QMASS1), (8) first quadrupole ion deflector (QDF1), (9) second octapole ion beam guide (OPIG2), (10) second quadrupole ion deflector (QDF2), (11) second quadrupole mass filter (QMASS2), (12) channeltron with conversion dynode, (13) quartz window.

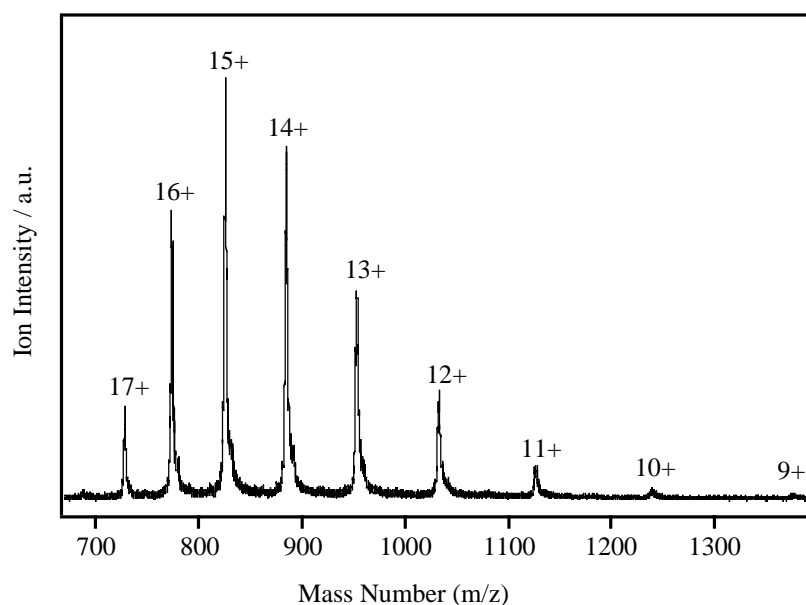
## 2. Experimental

Fig. 1 shows a schematic diagram of the apparatus consisting of an ESI source and a tandem mass spectrometer with octapole ion beam guides. Multiply-charged protein ions are produced by ESI of a dilute solution of cytochrome c (Sigma-Aldrich) in methanol-water (1:1 v/v) mixture including acetic acid (2.0%). Optimum intensity and stability of ion signals are obtained with a  $1.2 \times 10^{-4}$  M solution of cytochrome c. The electro spray needle is biased at +7 ~ +9 kV with respect to a platinum aperture of 0.1 mm in diameter located 15 – 20 mm from the needle tip. The platinum aperture is biased +150 ~ +350 V against the ground. A flow of 10 – 100 mL/s of dry nitrogen is maintained through the atmospheric pressure ion source. The flow continuously removes solvent vapor produced by the electro spray. Ions produced by the electro spray in the atmospheric region drift under the influence of the electric field towards the interface plate, and enter the interface region through a hole (4 mm in diameter) on the interface plate. The interface plate is heated up to about 350 K. Ions formed

at atmospheric pressure in the ESI source are admitted into the first vacuum chamber, which is evacuated by a 3000 L/s diffusion pump (ULVAC, ULK-10A). Typical pressure in the first chamber is  $2.0 \times 10^{-4}$  Torr. A beam of the ions then passes through a stainless-steel skimmer, and is focused by electrostatic lenses into the first-octapole ion beam guide (OPIG1) [30]. The OPIG is composed of eight molybdenum rods with 4 mm in diameter, which are evenly positioned on a circle of 16 mm in diameter. High transmission efficiency for slow ions is accomplished by applying a radio frequency (RF) field to the rods. The OPIG1 is connected directly to the first quadrupole mass spectrometer (QMASS1) (ABB EXTEL, 664901) in the second chamber evacuated by a 2000 L/s diffusion pump (Edwards, Diffstak 250/2000C). Typical pressure in the second chamber is  $5.0 \times 10^{-6}$  Torr. The first quadrupole ion deflector (QDF1) deflects the mass-selected ion beam emerging from QMASS1. The ions are admitted into the second-octapole ion beam guide (OPIG2) with a length of 88 cm, which is placed in the third chamber evacuated with a 400 L/s turbo molecular pump (SEIKO SEIKI, STP-400). Typical pressure in the third chamber is  $2.0 \times 10^{-7}$  Torr. After passing through OPIG2, the parent and the product ions are deflected by the second quadrupole ion deflector (QDF2), and are admitted into the second quadrupole mass spectrometer (QMASS2) (ABB EXTEL, 652601). The ions are mass-selected and detected by a channeltron electron multiplier equipped with an ion-conversion dynode. Depletion yield of the parent cluster ions in OPIG2 is measured with irradiating a photolysis laser. The laser beam is introduced into the guide collinearly and counterpropagatedly with the ion beams. We use the second ( $18800 \text{ cm}^{-1}$ ) or third ( $28200 \text{ cm}^{-1}$ ) harmonic of a YAG laser as the photolysis laser. Relative photodepletion cross section,  $\sigma_{\text{rel}}$ , is determined by

$$\sigma_{\text{rel}} = \ln(I_{\text{off}}/I_{\text{on}})/\phi, \quad (1)$$

where  $\phi$  is the photon fluence,  $I_{\text{on}}$  and  $I_{\text{off}}$  are the signal intensities of ions with and without irradiating the photolysis laser, respectively.



**Fig. 2.** Typical mass spectrum of multiply-charged cytochrome c ions produced by ESI as a function of mass/charge ratio,  $m/z$ .

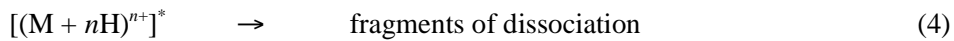
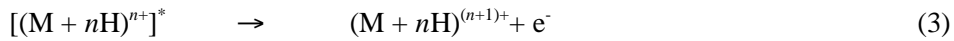
### 3. Results and Discussion

#### 3.1. Products of Photo-Induced Reactions.

Typical mass spectrum of multiply-charged cytochrome c ions,  $(M + nH)^{n+}$ , produced by ESI is presented in Fig. 2 as a function of mass/charge ratio,  $m/z$ . The observed mass spectrum consists of multiply-charged ions ranging from the  $n = 9$  to 17 charge states. Intensity and mass distribution of the ionic species produced by ESI depend strongly on the electric field strength of the high-pressure zone in the first chamber [31]. High electric field increases the kinetic energy of ion collisions with the background gas. By optimization of the electric field, ions of specific charge states are produced efficiently. With increasing the electric field, intensities of smaller charge states are enhanced. In the present study, we do not observe metastable decomposition of the ions between the initial mass selection and the final detection.

The photo-induced reactions of the charge-state selected cytochrome c ions are investigated at 18800 and 28200  $\text{cm}^{-1}$ . All charge states examined exhibit relatively strong photodepletion in both excitations. The absorption bands in visible and UV regions of cytochrome c in solution are ascribed to the  $\pi\pi^*$  transition of heme. The spectrum exhibits the absorption bands of moderate intensity in visible region called as Q bands ( $\epsilon \sim 2 \times 10^4$ ) and an extremely strong absorption band at  $\sim 25000 \text{ cm}^{-1}$ , which is called as Soret band ( $\epsilon \sim 3 \times 10^5$ ) [32]. The photo-induced reactions of the ions are examined by the excitation of these transitions in heme.

The product ions are considered to be generated through the following processes; photoexcitation of heme in the protein ions (eq. 2), subsequent photoionization (eq. 3), or photodissociation (eq. 4), as follows,



where  $[(M + nH)^{n+}]^*$  represents cytochrome c ions in the excited states. In this scheme, the photoionization (eq. 3) competes with the dissociation (eq. 4). In relation to the third process, a number of fragments have been observed via the cleavage of polypeptide chains in the collision-induced dissociation (CID) of protein ions [19,26,29]. We would also expect to observe the similar fragmentation process for the photolysis of protein ions. In contradiction with this expectation, the fragment ions are not detected with sufficient intensity except for the aforementioned multiply-charged ions,  $(M + nH)^{(n+1)+}$ . However, the results on the cross section of the photodepletion indicate the contribution of third process as mentioned later.

In order to analyze the photodissociation process, we examine the branching fraction for the ionization,  $R_{\text{ion}}$ , as

$$R_{\text{ion}} = I_{\text{pro}}[(M + nH)^{(n+1)+}] / I_{\text{dep}}[(M + nH)^{n+}] \quad (5),$$

where  $I_{\text{pro}}[(M + nH)^{(n+1)+}]$  is the ion intensity of the product ion,  $(M + nH)^{(n+1)+}$ , whereas  $I_{\text{dep}}[(M +$

$nH)^{n+}$ ] is the depletion ratio of the parent ion. Fig. 3 shows the branching fractions of the photoionization process plotted as a function of charge,  $n$ . Open squares and filled circles indicate the branching fractions determined at 18800 ( $47 \text{ mJ cm}^{-2} \text{ pulse}^{-1}$ ) and  $28200 \text{ cm}^{-1}$  ( $7.8 \text{ mJ cm}^{-2} \text{ pulse}^{-1}$ ), respectively. As shown in the figure, the branching fractions in both excitations decrease monotonously with increasing the charge up to  $n = 16$ . The branching fractions are not dependent on the laser fluence in both excitations. Smith and coworkers have reported the CID experiments of multiply-charged cytochrome c ions [26-28]. They have observed both charge transfer (CT, leading to loss of charge) and charge-stripping (CS, increase of charge by electron ejection) in addition to the CID process to produce singly charged fragments. CID has been found to be dominant for the +14 to +19 ions, while the CT and CS processes are dominant for  $n = 9 - 12$ . The present

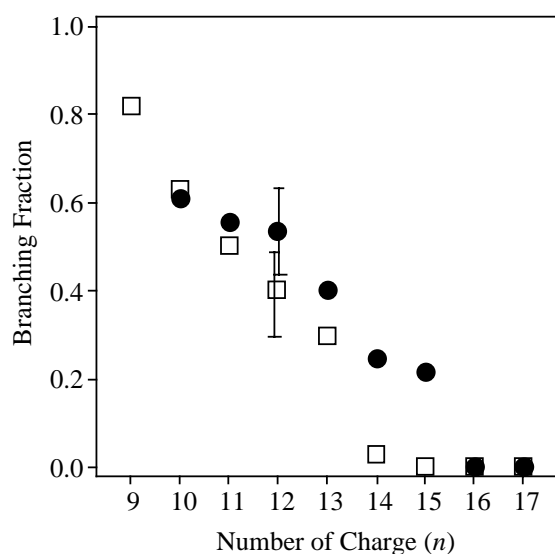


**Fig. 3.** Branching fractions for the photoionization of multiply-charged cytochrome c ions as a function of charge. Open squares and filled circles show the branching fractions determined with photolysis of the second ( $18800 \text{ cm}^{-1}$ ) or the third harmonic ( $28200 \text{ cm}^{-1}$ ) of YAG lasers, respectively.

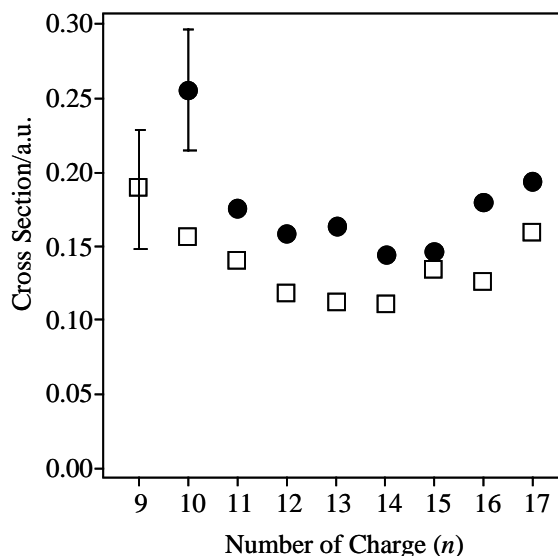


**Fig. 4.** Cross sections for the photodepletion of multiply-charged cytochrome c ions as a function of charge. Open squares and filled circles indicate the relative cross sections determined with photolysis of the second ( $18800 \text{ cm}^{-1}$ ) or the third harmonic ( $28200 \text{ cm}^{-1}$ ) of YAG lasers, respectively.

results are similar to those of the CID experiments. In Fig. 4, the relative cross sections of the photodepletion of multiply-charged cytochrome c ions,  $(M + nH)^{n+}$ , ( $n = 9 - 17$ ) are plotted as a function of the charge. Open squares and filled circles indicate the cross sections determined at  $18800 \text{ cm}^{-1}$  ( $47 \text{ mJ cm}^{-2} \text{ pulse}^{-1}$ ) and  $28200 \text{ cm}^{-1}$  ( $7.8 \text{ mJ cm}^{-2} \text{ pulse}^{-1}$ ), respectively. As shown in the figure, the cross sections decrease gradually with increasing charges from  $n = 9$  to 12, while they increase gradually for  $n = 15 - 17$  in both excitations.

Fig. 5 shows the laser fluence dependence on the photodepletion yield of cytochrome c ions ( $n = 14$ ) examined at  $28200 \text{ cm}^{-1}$ . The depletion yield increases in proportion to the 2.2 power of the laser fluence; the reactions proceed via two-photon excitation. The photodepletion yield at  $18800 \text{ cm}^{-1}$  also increases in proportion to the 2~3 power of the laser fluence. In the present experiment, the pulse width of the laser is  $5 \times 10^{-9} \text{ s}$ , and the photon fluxes of the photolysis laser are  $2.8 \times 10^{24} \text{ cm}^{-2} \text{ s}^{-1}$  and

$2.6 \times 10^{25} \text{ cm}^{-2} \text{ s}^{-1}$  at  $28200$  and  $18800 \text{ cm}^{-1}$ , respectively. The ionization cross sections from the  $\pi\pi^*$  excited states are assumed to be the same as that for the transition from the ground state; they are  $1.1 \times 10^{-13} \text{ cm}^2$  and  $7.6 \times 10^{-15} \text{ cm}^2$  at  $28200 \text{ cm}^{-1}$  and  $18800 \text{ cm}^{-1}$ , respectively. By using these values, the rate constants for the ionization from the excited states are estimated as  $3.0 \times 10^{11} \text{ s}^{-1}$  and  $2.0 \times 10^{11} \text{ s}^{-1}$  at  $28200 \text{ cm}^{-1}$  and  $18800 \text{ cm}^{-1}$ , respectively. Lifetime of the  $\pi\pi^*$  excited state of iron porphyrins in solution has been reported as 25-50 ps [33]. The rate constants of the ionization are nearly the same order as that of the decay process. Therefore, the observed photoionization of cytochrome c ions is ascribed to the multiphoton excitation of heme.

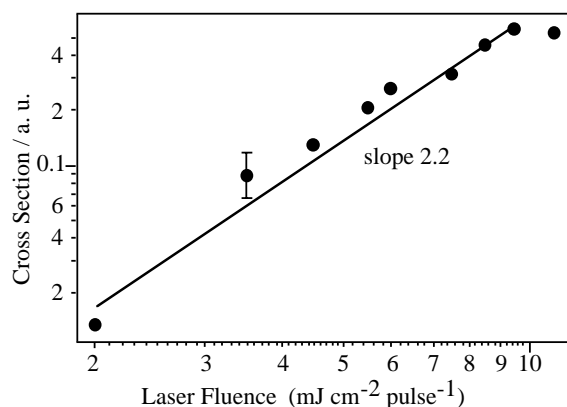


**Fig. 5.** Laser fluence dependence for the photodepletion of multiply-charged cytochrome c ions ( $n = 14$ ) at  $28200 \text{ cm}^{-1}$ . The depletion yield increases in proportional to the 2.2 power of the laser fluence.

### 3.2. Model calculation of photoionization

As mentioned in the previous section, the photoionization (eq. 3) at  $28200 \text{ cm}^{-1}$  proceeds via two-photon excitation of heme for  $n < 16$ . In order to clarify the origin of the size-dependence of the photoionization yield, we carry out the model calculations. Since the polypeptide in cytochrome c ions has positive charges, the photo-ejection of an electron (ionization) from heme takes place under the influence of Coulombic attractive potential. In a crude approximation, the upper limit of the excess energy,  $E_{\text{ex}}$ , in the photoionization can be defined as

$$E_{\text{ex}} = 2h\nu - \text{IP}_{\text{heme}} \quad (6),$$

where  $h\nu$  and  $\text{IP}_{\text{heme}}$  are the photon energy and the ionization potential of heme in cytochrome c ions. The photoionization may occur if the attractive potential becomes less than  $E_{\text{ex}}$ . It has been reported that heme iron in cytochrome c ions produced with ESI is the Fe (II) form [34,35], and thus, heme in multiply-charged cytochrome c ions is electrically neutral. Ionization potential (IP) of the gas-phase iron-porphyrins has been determined to be 6.06 eV (Fe (II) OEP) and 6.09 eV (Fe (III) CITPP) by the photoelectron spectroscopy [36] and photocurrent measurement [37], respectively. IP of heme in the ions may be roughly close to these values. Thus,  $E_{\text{ex}}$  in the two-photon ionization at  $28200 \text{ cm}^{-1}$  (6.99 eV) is estimated to be  $\sim 0.9 \text{ eV}$ . In the following sections, we calculate the attractive potentials with structural models and compare the results with the above  $E_{\text{ex}}$ .

#### 3.2.1. Sphere Model

In the first scheme, the Coulomb attractive potential is estimated by assuming that the shapes

of the protein ions are spheres. It is also assumed that the charges are distributed uniformly over the surface of the sphere. Based on these assumptions, the Coulomb potential energy on the surface of the sphere,  $U_{sp}$ , is expressed by

$$U_{sp} = - \frac{ne^2}{6\pi \epsilon_0 \epsilon_r r_n} \quad (7),$$

where  $n$  is the number of charges,  $\epsilon_r$  is the dielectric constant of protein to account for the shielding of the charges by protein itself, and  $r_n$  is the radius of the sphere for the protein ion with the number of charge  $n$ . As for the relative dielectric constant, Williams and coworkers have suggested the value of  $\sim 2.0$ , which is appropriate for the gas-phase cytochrome c ion [22]. X-Ray crystal structure coordinates and NMR solution structure coordinates, obtained from the Protein Data Bank, give a value for an effective radius of the sphere,  $r_n$ , as  $9.25 \text{ \AA}$  for the native conformations [38]. If the conformation of the gas-phase ions is the same as the native one,  $U_{sp}$  is calculated to be  $8.3 \text{ eV}$  for  $n = 16$ , which is much larger than  $E_{ex}$  ( $\sim 0.9 \text{ eV}$ ). This result suggests that the Coulomb potential energy is overestimated with this model. Jarrold and coworkers have examined the cross sections ( $S_n$ ) of cytochrome c ions in the gas phase as a function of charge by ion mobility measurements [23-25]. The effective radius,  $r_n = (S_n/4\pi)^{1/2}$ , for the gas-phase ions is obtained as  $14.7 \text{ \AA}$ . Using this value, the  $U_{sp}$  value is calculated to be  $5.2 \text{ eV}$  for  $n = 16$ , which is still larger than  $E_{ex}$ . Therefore, the arguments suggest that the conformation is quite different from sphere.

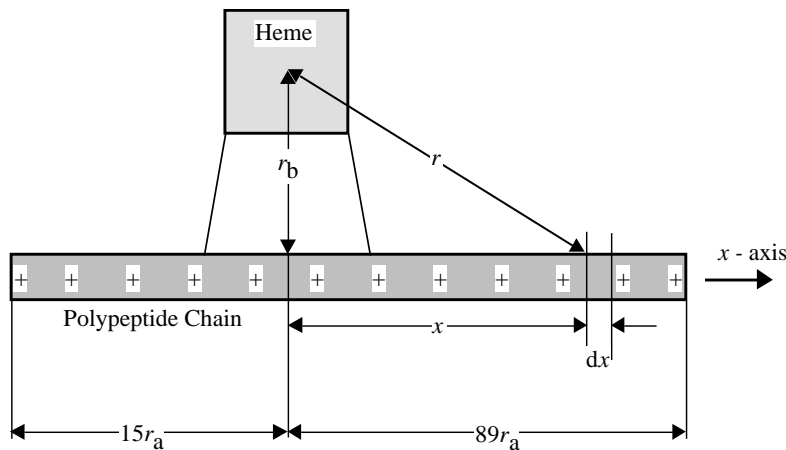


**Fig. 6.** Schematic of the scheme to calculate Coulomb potential at heme, by assuming that the polypeptide chain in the protein ions is a linear string, and that the charges are distributed uniformly over the polypeptide chain.

### 3.2.2. Linear string Model

The Coulomb attractive potential depends upon the conformation of polypeptide chain. Cytochrome c has no disulfide bridges and is relatively free to adopt conformations, which are quite different from the native conformation. In relation to this issue, the molecular dynamics simulations for cytochrome c ions have predicted that the geometries close to the native structure in solution are dominant for the low charge states ( $n = 3 - 5$ ), while extended conformations are dominant for the higher charge states ( $n = 7 - 20$ ) [23-25]. These results suggest that cytochrome c ions in the present experiments ( $n = 9 - 17$ ) are completely unfolded. Cytochrome c is composed of 104 residues. Heme

is covalently bound to cysteine 14 and cysteine 17. In native conformation, heme iron is bound to the nitrogen and sulfur atoms in histidine 18 and in methionine 80, respectively [38]. When cytochrome c unfolds, these ligands would dissociate from the iron. Thus, in the second model, the Coulomb attractive potential is estimated by assuming that the polypeptide chain in the protein ions is a linear string, and that the charges are distributed uniformly over the polypeptide chain along the  $x$ -axis as shown in Fig. 6. Contribution of these charges to the Coulomb potential per a unit length,  $dU_{\text{string}}$ , is estimated by the equation,

$$dU_{\text{string}} = - \frac{\rho e}{4\pi\epsilon_0\epsilon_r} \frac{dx}{r} \quad (8)$$

where  $\rho$  is the charge density distributed over the residues in the polypeptide chain of the same average size.  $\rho$  is given by

$$\rho = \frac{ne}{104r_a} \quad (9)$$

where  $n$  is the number of the charges,  $r_a$  is the length of polypeptide chain per one residue, which is equal to 3.6 Å [39,40]. The distance between heme and the charges,  $r$ , is given by

$$r = \sqrt{x^2 + r_b^2} \quad (10)$$

where  $r_b$  is the distance between heme and the polypeptide chain. Because heme is bound to the polypeptide chain with cysteine 14 and cysteine 17, the  $r_b$  value is equal to 9.27 Å. By the integration of  $dU_{\text{string}}$  along the  $x$ -axis, the Coulomb potential energy at heme,  $U_{\text{string}}$ , is expressed as

$$U_{\text{string}} = \int_0^{89r_a} dU_{\text{string}} + \int_0^{15r_a} dU_{\text{string}}. \quad (11)$$

The calculated  $U_{\text{string}}$  values are plotted in Fig. 7 as a function of  $n$ . The  $U_{\text{string}}$  value for  $n = 16$  is given as 0.89eV and is almost equal to the excess energy,  $E_{\text{ex}}$ . For  $n < 16$ , the  $U_{\text{string}}$  values become lower than  $E_{\text{ex}}$  and the ionization is expected to occur. These results are consistent with the present experimental findings; the critical number of charge,  $n$ , for the ionization is 16. Therefore, the calculations indicate that the shapes of the protein ions are similar to the linear string. Although the present calculations use the oversimplified models, the results are consistent with the observed behaviors for the photoionization of cytochrome c ion.

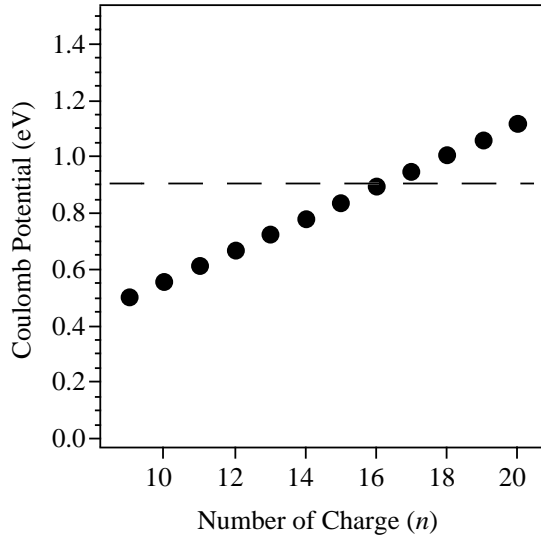


**Fig. 7.** Coulomb attractive potentials at heme, which are contributed by the charges on the linear polypeptide chain, are plotted with filled circles. The broken line indicates the excess energy,  $E_{\text{ex}}$ , of two-photon ionization at  $28200 \text{ cm}^{-1}$ .

### 3.2.3. Cleavage of polypeptide chain

As mentioned in the previous section, the cross sections increase gradually for  $n = 15 - 17$  in both excitations, though the photoionization yields decrease monotonously in this size range. Although no dissociation products are observed in the present experiment, these results clearly suggest the occurrence of the dissociation of polypeptide chain as in the case of CID experiments [26, 27]. In order to confirm the presence of the dissociation channel, we examine the repulsive interaction in the multiply-charged polypeptide chain, which may enhance the dissociation process. Relating to this issue, Rockwood and coworkers have estimated the activation energy for the dissociation of gas-phase protein ions by assuming a “charges on a string” model [41]. Using their model, we also estimate an energy release upon dissociation. In the present calculations, the polypeptide chain in the protein ions is assumed as a linear string, in which the charges are distributed uniformly over the residues in the chain. The Coulomb repulsive potential between the two fragment ions,  $U_{\text{rel}}$ , is estimated by

$$U_{\text{rel}} = -\frac{\rho^2}{4\pi\epsilon_0\epsilon_r} \int_0^{r_1} \int_0^{r_2} \frac{dx_1 dx_2}{x_1 x_2} \quad (12)$$

where  $r_1$  and  $r_2$  are the length of peptide chains for two fragment ions. The maximum value for the repulsion potential,  $U_{\text{rel}(\text{max})}$ , is obtained when the cleavage occurs at the bond in the middle of peptide chain;  $r_1$  is equal to  $r_2$ . For  $n = 17$ , the  $U_{\text{rel}(\text{max})}$  value is estimated to be 3.83 eV and suggest the enhancement of the bond dissociation. The gradual increase of the photodepletion cross section with increasing  $n$  from 15 to 17 as seen in Fig. 4 may be ascribed to the increase of the dissociation yield as a result of the Coulomb repulsion. At the moment, we have no clear explanation for the absence of the fragmentation products. One of the possible reasons may be the broadening of the kinetic-energy distribution of fragment ions in OPIG2, which may cause as a result of the energy release by Coulomb repulsion upon dissociation and induces the reduction of the transmission efficiency of QDF2.

#### 4. Conclusions

We have constructed the photodissociation mass spectrometer equipped with electrospray ionization source. Using this apparatus, photo-induced reactions of multiply-charged cytochrome c ions,  $n = 9 - 17$ , have been investigated at 28200 and 18800  $\text{cm}^{-1}$ . The mass spectra of the photoproducts show that the ionization occurs dominantly for the lower charged states. The laser fluence experiments indicate that the ionization at 28200  $\text{cm}^{-1}$  is two-photon process, while more photons are required for the excitation at 18800  $\text{cm}^{-1}$ . A drastic decrease for the ionization yields is observed with increasing the charge states,  $n$ . This change is interpreted by the ionization of heme under the influence of the Coulomb attractive potential in the polypeptide chain. Model calculations for the Coulomb potential suggest that structure of the polypeptide chain is completely elongated.

#### Acknowledgements

This work is partially supported by the Grant-in-Aid (Grants #11304042) from the Ministry of Education, Science, Sports and Culture of Japan, and by the Grant-in-Aid for Scientific Research (Grants #11740326, and #13640512) and a research grant for the future program from Japan Society for Promotion of Science. KF is also grateful to the Hyogo Science and Technology Association for partial financial supports.

#### References

- [1] M. T. Bowers, A. G. Marshall, F. W. McLafferty, *J. Phys. Chem.* 100 (1996) 12897.
- [2] H. Haberland (Ed.), *Clusters of Atoms and Molecules*, Vol. I and II, Springer-Verlag, 1994, and reference there in.
- [3] A. W. Castleman, Jr., K. H. Bowen, *J. Phys. Chem.* 100 (1996) 12911.
- [4] M. A. Duncan (Ed.), *Advances in Metal and Semiconductor Clusters*, JAI Press Inc., 2000, and references there in.
- [5] K. Fuke, K. Hashimoto, S. Iwata, *Adv. Chem. Phys.* 110 (1999) 431, and references there in.
- [6] Y. Ohshima, O. Kajimoto, K. Fuke, in Y. Haas (Ed.), *Electron Transfer in Chemistry*, Wiley-VCH, in press.
- [7] M. Sanekata, F. Misaizu, K. Fuke, *J. Chem. Phys.* 100 (1994) 1161.
- [8] (a) R. Takasu, F. Misaizu, K. Hashimoto, K. Fuke, *J. Phys. Chem. A* 101 (1997) 3078.  
(b) R. Takasu, H. Ito, K. Nishikawa, K. Hashimoto, R. Okuda, K. Fuke, *J. El. Spectros. Relat. Phenom.* 106 (2000) 127.
- [9] (a) S. Nonose, T. Taguchi, F. Chen, S. Iwata and K. Fuke, *J. Phys. Chem. A*, **106** 5242 (2002).  
(b) S. Nonose, T. Taguchi, K. Mizuma and K. Fuke, *Europ. Phys. J. D*, **9** 309 (1999).  
(c) N. Okai, A. Takahata, M. Morita, S. Nonose, and K. Fuke, *J. Phys. Chem. A*, in press.
- [10] C. Nitsch, Chr. Hüglin, I. V. Hertel, C. P. Schulz, *J. Chem. Phys.* 101 (1994) 6559.
- [11] C. P. Schulz, C. Nitsch, *J. Chem. Phys.* 107 (1997) 9794.
- [12] P. Brockhaus, I. V. Hertel, C. P. Schulz, *J. Chem. Phys.* 110 (1999) 393.
- [13] R. B. Cole (Ed.), *Electrospray Ionization Mass Spectrometry*, Wiley, New York, 1997.

- [14] C. M. Whitehouse, R. N. Dreyer, M. Yamashita, J. B. Fenn, *Anal. Chem.* 57 (1985) 675.
- [15] (a) S. Nonose, H. Tanaka, N. Okai, T. Shibakusa, K. Fuke, *Europ. Phys. J. D* 20 (2002) 619.  
(b) S. Nonose, S. Iwaoka, H. Tanaka, N. Okai, T. Shibakusa, K. Fuke, *Europ. Phys. J. D* 24 (2003) 335.
- [16] T. G. Spence, T. D. Burns, G. B. Guckenberger, L. A. Posey, *J. Phys. Chem.* 101 (1997) 1081.
- [17] C. J. Thompson, J. Husband, F. Aguirre, R. B. Metz, *J. Phys. Chem.* 104 (2000) 8155.
- [18] X.-B. Wang, L.-S. Wang, *J. Chem. Phys.* 111 (1999) 4497.
- [19] R. A. Zubarev, D. M. Horn, E. K. Fridriksson, N. L. Kelleher, N. A. Kruger, M. A. Lewis, B. K. Carpenter, F. W. McLafferty, *Anal. Chem.* 72 (2000) 563.
- [20] F. W. McLafferty, Z. Guan, U. Haupts, T. D. Wood, N. L. Kelleher, *J. Am. Chem. Soc.* 120 (1998) 4732.
- [21] P. D. Schnier, D. S. Gross, E. R. Williams, *J. Am. Chem. Soc.* 117 (1995) 6747.
- [22] R. A. Jockusch, P. D. Schnier, W. D. Price, E. F. Srittmatter, P. A. Demirev, R. Williams, *Anal. Chem.* 69 (1997) 1119.
- [23] M. F. Jarrold, *Acc. Chem. Res.* 32 (1999) 360.
- [24] Y. Mao, J. Woenckhaus, J. Kolafa, M. A. Ratner, M. F. Jarrold, *J. Am. Chem. Soc.* 121 (1999) 2712.
- [25] Y. Mao, M. A. Ratner, M. F. Jarrold, *J. Am. Chem. Soc.* 123 (2001) 6503.
- [26] R. D. Smith, C. J. Barinaga, H. R. Udseth, *J. Phys. Chem.* 93 (1989) 5019.
- [27] R. D. Smith, C. J. Barinaga, *Rapid Commun. Mass Spectrom.* 4 (1990) 54.
- [28] J. Martin, E. Quirke, in K. M. Kadish, K. M. Smith, R. Guillard (Eds.), *Porphyrin handbook*, Vol. 7, Sec. 54, pp 409 - 412, Academic Press, San Diego, 2000.
- [29] Q. Wu, S. Van Orden, X. Cheng, R. Bakhtiar, R. D. Smith, *Anal. Chem.* 67 (1995) 2498.
- [30] E. Teloy, D. Gerlich, *Chem. Phys.* 4 (1974) 417.
- [31] R. D. Smith, J. A. Loo, C. J. Barinaga, C. G. Edmonds, H. R. Udseth, *J. Am. Soc. Mass Spectrom.* 1 (1990) 53.
- [32] M. Gouterman, *J. Mol. Spectroscopy*, 6 (1961) 138.
- [33] K. Kalyanasundaram, *Photochemistry of Polypyridine and Porphyrin Complexes*, Academic Press, London, 1992, pp493-534.
- [34] Y.-Ti. Li, Y.-L. Hsiah, J. D. Henion, B. Ganem, *J. Am. Soc. Mass Spectrom.* 4 (1993) 631.
- [35] G. J. Van Berkel, F. Zhou, J. T. Aronson, *Int. J. Mass Spectrom. Ion Proc.* 162 (1997) 55.
- [36] S. Kitagawa, I. Morishima, T. Yonezawa, N. Sato, *Inorg. Chem.* 18 (1979) 1349.
- [37] Y. Nakato, K. Abe, H. Tsubomura, *Chem. Phys. Lett.* 39 (1976) 358.
- [38] <http://www.rcsb.org/pdb/>.
- [39] G. E. Schulz, R. H. Schirmer, *Principles of Protein Structure*, Springer-Verlag, 1980.
- [40] R. W. Vachet, A. D. Winders, G. L. Glish, *Anal. Chem.* 68 (1996) 522.
- [41] A. L. Rockwood, M. Busman, R. D. Smith, *Int. J. Mass Spectrom. Ion Proc.* 111 (1991) 103.